How to cite: Angew. Chem. Int. Ed. 2023, e202313833
doi.org/10.1002/anie.202313833

Solar Cells

Directional Defect Management in Perovskites by In Situ Decom-position of Organic Metal Chalcogenides for Efficient Solar Cells

Guan-E Wang[+], Guo-Bin Xiao[+], Cong-Ping Li, Zhi-Hua Fu, Jing Cao, and Gang Xu**

Abstract: Directional defects management in polycrystalline perovskite film with inorganic passivator is highly demanded while yet realized for fabricating efficient and stable perovskite solar cells (PSCs). Here, we develop a directional passivation strategy employing a two-dimensional (2D) material, Cu-(4-mercaptophenol) (Cu-HBT), as a passivator precursor. Cu-HBT combines the merits of the targeted modification from organic passivator and excellent stability offered by inorganic passivator. Featuring with dense organic functional motifs on its surfaces, Cu-HBT has the capability to "find" and fasten to the Pb defect sites in perovskites through coordination interactions during a spin-coating process. During subsequent annealing treatment, the organic functional motifs cleave from Cu-HBT and convert in situ into *p*-type semiconductors, Cu_2S and PbS. The resultant Cu_2S and PbS not only serve as stable inorganic passivators on the perovskite surface, significantly enhancing cell stability, but also facilitate efficient charge extraction and transport, resulting in an impressive efficiency of up to 23.5 %. This work contributes a new defect management strategy by directionally yielding the stable inorganic passivators for highly efficient and stable PSCs.

Organic-inorganic metal halide perovskite semiconductor materials possess many attractive optoelectronics properties, such as tunable band gap, high absorption coefficient, low trap density as well as long intrinsic carrier recombination lifetime, which are suitable for the application of photovoltaic filed.[1] The power conversion efficiency (PCE) record of perovskite solar cells (PSCs) has been continually broken over the past decade and achieved a certified PCE of 26.1 %.[2] This remarkable progress positions PSCs as promising candidates for high-efficiency and ultralow-cost photoelectric conversion equipment in the future.[3] However, the large number of defects could inevitably yield in perovskite film during the solution processed process, impeding the fabrication of efficient and stable PSCs. On one hand, the photogenerated electrons (or charges) could be captured or trapped when approaching these defects, and thus reducing the performance of PSCs.[4] On the other hand, the charges trapped in these defects lead to the reduction of Pb^{2+} and the oxidation of I^-, leading to the degradation of perovskite.[5] Furthermore, the defects also instigate ion migration, the escape of organic cation, and the penetration of moisture and oxygen, all of which accelerate the decomposition of perovskite.[6]

The passivation of defects in perovskite materials has been a subject of intensive research, involving both organic and inorganic materials.[7] Organic materials, like D-4-tert-butylphenylalanine, passivate the defects through coordination, electrostatic interactions and other weak interactions.[8] This unique characteristic allows organic passivators to selectively bond to defective sites on the perovskite surface, as these passivators exhibit migratory behavior due to their relatively weak interactions. In contrast, inorganic materials, such as $PbSO_4$, $Pb_3(PO_4)_2$ and chlorinated graphene oxide, can covalently bond to the defects and provide much better stability.[9] However, inorganic passivators normally form a coating layer on the whole perovskite surface, lacking the ability to selectively address specific defect sites. How to directionally manage the defects in perovskite film by the inorganic passivators is still a pending question.

To address this question, a type of newly emerging two-dimensional (2D) materials, organic metal chalcogenides (OMCs), have attracted our interests.[10] OMCs structurally feature with a metal chalcogenide inorganic layer sandwiched by covalently bonded organic functional motifs. Capitalizing on this distinctive structure, OMCs may offer the potential to amalgamate the advantages of both organic and inorganic passivators to solve above-mentioned issues.

[*] Prof. G.-E Wang,[+] Dr. Z.-H. Fu, Prof. G. Xu
State Key Laboratory of Structural Chemistry, Fujian Provincial Key Laboratory of Materials and Techniques toward Hydrogen Energy, Fujian Institute of Research on the Structure of Matter, Chinese Academy of Sciences (CAS)
155 Yangqiao Road West, Fuzhou, Fujian, 350002 (China)
E-mail: gxu@fjirsm.ac.cn

G.-B. Xiao,[+] C.-P. Li, Prof. J. Cao
State Key Laboratory of Applied Organic Chemistry, Key Laboratory of Nonferrous Metal Chemistry and Resources Utilization of Gansu Province, College of Chemistry and Chemical Engineering, Lanzhou University
Lanzhou, Ganshu, 730000 (China)
E-mail: caoj@lzu.edu.cn

Prof. G. Xu
Fujian Science & Technology Innovation Laboratory for Optoelectronic Information of China
Fuzhou, Fujian, 350108 (China)

[+] These authors contributed equally to this work.

With elaborative designs, the dense organic motifs on OMCs can help to directionally connect to the defective surfaces during a spin-coating process. During subsequent annealing steps, the organic motifs cleave from OMCs and vaporize into the surrounding environment, leading to the in situ formation of inorganic passivators on the defective surface. Notably, in order to optimize the cell performance, the resultant inorganic passivator is better to be a semiconductor that matches the energy level of the perovskite.

Considering these considerations, one of OMCs, Cu-(4-mercaptophenol) (Cu-HBT),[11] constructed by phenol group covalently grafting {CuS} layer as depicted in Figure 1a was selected due to: 1) the favored interaction between phenolic hydroxyl and Pb defect sites of perovskite; 2) easy cleavage of the C–S bond between phenol and {CuS} layer, and high volatility of the cleaved phenol; 3) in situ generated passivators, like Cu_2S and PbS, are energy-favored *p*-type semiconductor for perovskite. As results, after treated by Cu-HBT with a thickness of 5 nm, PSCs remarkably enhanced their stability in resistance of the humidity, thermal and light due to the resultant Cu_2S and PbS inorganic passivators. Furthermore, Cu_2S and PbS facilitate the charge extraction and reduce the charge recombination, which increases the average efficiency by 1.8 % and reaches the best efficiency of 23.5 % for the modified PSCs.

Cu-HBT 2D material with thickness of ≈5 nm (Figure S1) was prepared through the reaction of 4-hydroxythiophenol and $CuCl_2 \cdot 2H_2O$ (additional details see Supporting Information).[11] The structure of Cu-HBT reveals that each Cu^+ coordinates with three S atoms, and reciprocally, each S atom coordinates with three Cu^+ ions, forming a graphene-like structure (as illustrated in Figure S2). Phenol functional motifs are covalently connected to {CuS} layer through C–S covalent bonds. This structure was confirmed by Powder X-ray diffraction (PXRD) analysis (Figure S3). For the preparation of Cu-HBT dispersion, Cu-HBT dispersed into chlorobenzene with the optimized concentration of 2.5 mg/mL. Subsequently, this dispersion was spin-coated on perovskite film and heated at 150 °C for 10 minutes to accomplish the in situ generation of inorganic passivator and fabrication of PSCs. Scanning electron microscopy (SEM) images (as shown in Figure 1b, S4 and S5) and elemental distribution analysis (as depicted in Figure S6) confirm the uniform dispersion of Cu-HBT on the surface of perovskite surface.

To probe the function way of Cu-HBT on perovskite surface, the Fourier transform infrared Spectroscopy (FTIR) were performed and presented in Figure 1c and S7. For the Cu-HBT-modified perovskite sample, the C–C stretching vibration peak of phenyl in 4-mercaptophenol at 1590 cm^{-1}, 1488 cm^{-1} and 1430 cm^{-1}, the O–H bending vibration peak at 1358 cm^{-1}, the C–O stretching vibration peak at 1249 cm^{-1} and the C–S stretching vibration peak at 1104 cm^{-1} are clearly observed. Compared to the pure Cu-HBT sample, the shift of these peaks suggests that Cu-HBT is chemically anchored to the perovskite surface. Particu-

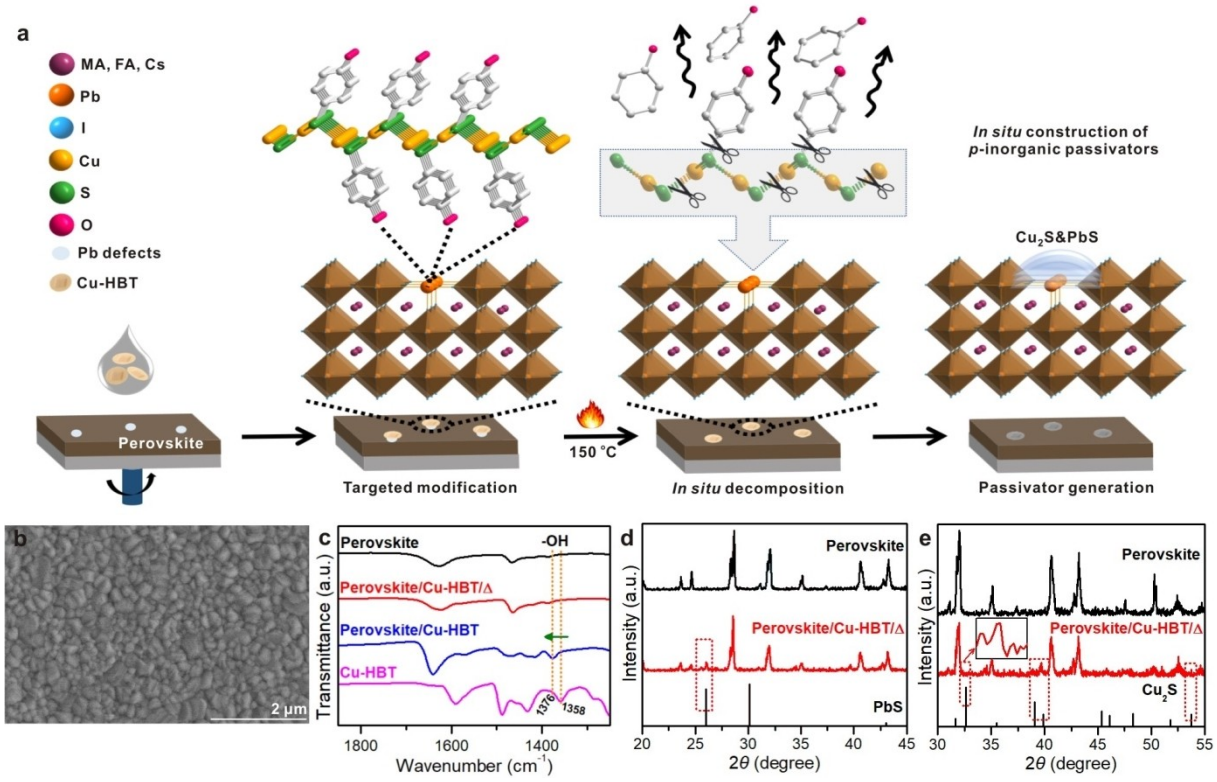

Figure 1. (a) Scheme illustration of directional Pb defects management strategy treated by Cu-HBT. (b) SEM image of perovskite modified by Cu-HBT with thermal treatment. (c) FTIR spectra of perovskite, Cu-HBT, perovskite modified by Cu-HBT before and after thermal treatment. (d–e) Enlarged XRD pattern of perovskite, Cu-HBT modified perovskite with thermal treatment.

larly, the shift of O–H bending vibration peak from 1358 cm^{-1} to 1376 cm^{-1} for Cu-HBT-modified perovskite sample, indicating that the Cu-HBT might be anchored to the defective sites of perovskite surface through the Pb–O coordination function (Figure 1c). Upon subjecting the sample to heating treatment, the disappeared FTIR and Raman peaks (Figure S7 and S8) corresponding to organic functional motifs indicate the removal of ligands. Although the Cu-HBT remains stable up to 260 °C, when mixed with perovskite, the decomposition of the Cu-HBT is promoted and begins at a lower temperature (approximately 140 °C) (Figure S9). This could be attributed to the effect of interfacial function of Cu-HBT and perovskite to facilitate the thermal decomposition of Cu-HBT. Additionally, the PXRD results also reveal that after Cu-HBT calcination at 300 °C, the organic ligands decompose (Figure S10).

X-ray photoelectron spectroscopy (XPS) measurements confirms that the remained Cu and S elements on perovskite defect sites maintains their original valence states (Figure S11). The shift of S and Pb peaks in the Cu-HBT modified sample proved that the S in Cu-HBT can interact with Pb in perovskite. The similar UV/Vis spectra suggests that the modified film does not alter the crystallographic structure of perovskite (Figure S12). PXRD tests were performed to characterize the structural composition of the inorganic phase after reaction. As shown in Figures 1d–e and S13, the phase of Cu_2S (PDF#72-1071) and PbS (PDF#05-0592) can be observed after heating treatment. Time of flight secondary ion mass spectrometry (TOF-SIMS) was tested to probe the chemical compositions throughout the film after thermal treatment. PbS^+ and Cu_2S^+ were mainly located on the surface of the perovskite film (Figure 2a, d and f). Meanwhile, PbI^+ also exhibited the highest content on the surface of perovskite film (Figure 2b and c), similar to that reported in the literature. The results are consistent with the corresponding TOF-SIMS 3D tomography (Figure 2e and g). Above results suggest that the reaction of released Cu, S ions and the Pb defects in perovskite might lead to the in situ formation of Cu_2S and PbS.

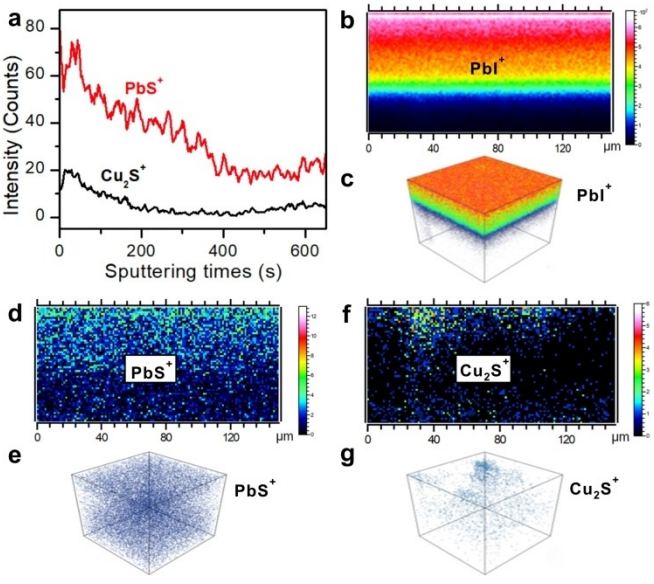

Figure 2. (a) Fragments distribution in Cu-HBT modified perovskite film after thermal treatment. TOF-SIMS results of PbI^+ (b–c), PbS^+ (d–e) and Cu_2S^+ (f–g) of perovskite film modified by Cu-HBT after thermal treatment.

The alignment of energy levels of passivators with the valence-band level of perovskite should be a critical factor to effectively extract the photogenerated holes. As shown in Figure 3a, the energy levels of Cu_2S and PbS are −5.1 and −5.2 eV,[12] respectively, slightly higher than the valence band of perovskite. This energy offset facilitates the efficient extraction of holes at the interface. To verify this hypothesis, time-resolved and steady state photoluminescence (PL) characterizations were performed. As shown in Figure 3b, the modified perovskite reveals the reduced decay time with 76.3 ns compared to the pure perovskite film (135.5 ns). This reduction in decay time suggests that Cu_2S and PbS passivators can accelerate the interfacial charge extraction. These results were further confirmed by the reduced intensity in steady-state PL for the treated perovskite (Figure S14).

Electrochemical impedance spectroscopy (EIS) tests were also prepared to assess the interfacial charge transport behavior by introducing the Cu_2S and PbS passivators. As shown in Figure 3c–d, Cu_2S and PbS passivated device exhibits higher interfacial recombination resistance (R_{rec}) and lower transfer resistance (R_{tr}) compared to the pristine device. These results indicate that Cu_2S and PbS passivators facilitate the efficient charge transport and reduce the interface charge recombination. Moreover, the Mott–Schottky (M–S) analyses were employed to assess the interfacial charge density and built-in-potential (V_{bi}) at interface between perovskite and hole transport material.[13] As demonstrated in Figure 3e, the slope observed in the modified perovskite devices is larger than that in pristine devices in M–S plots, which indicated a lower charge density in modified perovskite devices interface. In other words, charge recombination and surface defects are reduced after modified by Cu-HBT.[14] Additionally, the larger V_{bi} of modified perovskite devices, as compared to pristine devices from the intercept, suggests improved hole extraction properties. These findings are consistent with the result of time-resolved PL measurement and energy levels diagram. Space charge limited current (SCLC) measurements reveal that the modified perovskite film displays the obviously reduced trap-state density (3.26×10^{14} cm^{-3}) than that of pure perovskite film (1.01×10^{15} cm^{-3}) (Figure 3f). This implies that PbS and Cu_2S effectively passivate the interfacial defect sites of the perovskite film, promoting the efficient charge transport and reducing the interfacial charge recombination, probably enhancing the cell performance of PSCs.

The PSCs devices based on the architecture of FTO/ZnO-MgO-EA^+[15]/mesoporous TiO_2/perovskite/Spiro-OMeTAD/Au (Figure S15) were fabricated to assess the passivating effect of Cu-HBT on the cell performance. In this configuration, the perovskite formula employed a mixed cationic structure of $Cs_{0.05}(MA_{0.17}FA_{0.83})_{0.95}Pb(I_{0.83}Br_{0.17})_3$. As illustrated in Figure 3g and summarized in Tables S1–S2, the

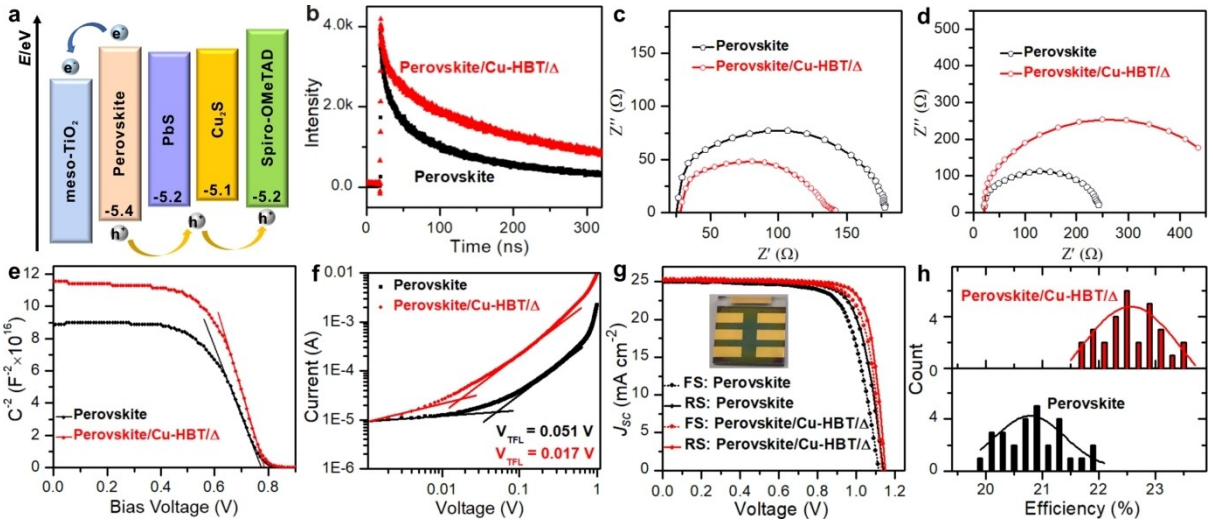

Figure 3. (a) Energy levels of perovskite, PbS, Cu_2S and Spiro-OMeTAD. (b) Time-resolved PL spectra of pristine perovskite and treated by Cu-HBT after thermal treatment. Nyquist plots of perovskite and Cu-HBT-modified perovskite after thermal treatment measured in a bias potential of 0 V (c) and 0.9 V (d). (e) Mott–Schottky plots of PSCs with perovskite and Cu-HBT modified perovskite after thermal treatment. (f) Space-charge-limited current (SCLC) measurements of perovskite and Cu-HBT-modified perovskite after thermal treatment. (g) Best *J–V* data tested in reverse (RS) and forward (FS) scans of PSCs of pristine PSC device and treated by Cu-HBT after thermal treatment. (h) Histograms of efficiencies among 30 cells without and with Cu-HBT-modified after thermal treatment.

highest efficiency of PSCs with Cu-HBT modification reaches 23.5 %, which is higher than that of the control devices with 21.9 % and is in a leading position in the field. The efficiency enhancement mainly attributed to improvements in V_{oc} (open-circuit voltage) and fill factor, both of which are indicative of more efficient interfacial charge transport. The calibrated current density obtained by incident photon-to-current conversion efficiency spectra (IPCE) also matches the current density obtained by *J–V* curves measurements (Figure S16). The efficiency distribution histogram for 30 devices is provided in Figure 3h. The average efficiency of the control devices is 20.8 % ± 1.1 %. while the average efficiency of the Cu-HBT treated devices increase to 22.6 % ± 1.0 %.

To demonstrate the efficacy of Cu_2S and PbS passivators in enhancing long-term stability, PSCs without encapsulated were subjected to stability testing. In order to exclude the influence of Spiro-OMeTAD on cell stability, we adopted the FTO/ZnO-MgO-EA^+/mesoporous TiO_2/perovskite/P3HT/Au structure to conduct the stability tests. As shown in Figure 4a, the treated perovskite film exhibited an increased water contact angle (98.1°) compared to the pristine perovskite film (62.3°). The moisture stability of PSCs was assessed under 45 % humidity at room temperature in air atmosphere. As demonstrated in Figure 4b, the treated device maintains 90 % of its original efficiency after 1000 hours, while the pristine device loses more than 50 % of its initial efficiency at the same condition.

Thermal and light stability are the main challenges in practical operation of PSCs. Therefore, the thermal and light stabilities of PSCs were investigated. As shown in Figures 4c and S17, the treated device reveals the excellent thermal stability, which maintains 90 % of its original efficiency after 1500 h at 85 °C with ~45 % humidity in air atmosphere. In

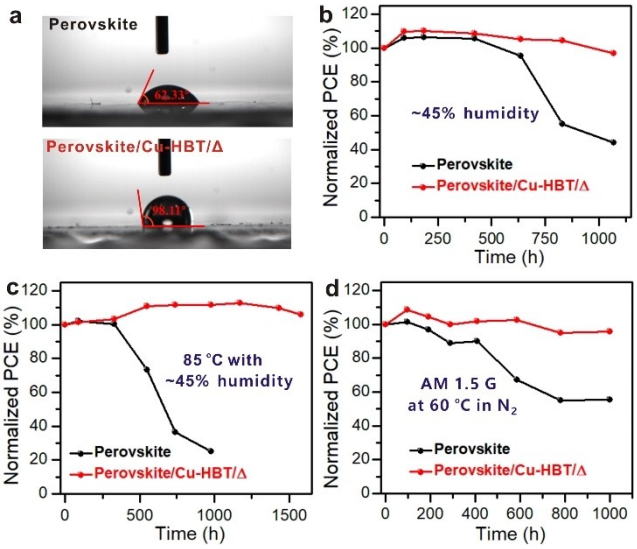

Figure 4. (a) Water contact angles of pristine perovskite and treated by Cu-HBT after thermal treatment. (b) Moisture stability tested with a humidity of about 45 %. (c) Thermal stability under 85 °C with ~45 % humidity in air atmosphere. (d) Thermal and light stability measured under AM 1.5 G illumination at 60 °C in N_2 atmosphere.

contrast, the pristine device loses more than 50 % of its initial efficiency after just 700 hours. The light stabilities of PSCs were conducted under AM 1.5 G illumination at 60 °C in N_2 atmosphere. As illustrated in Figure 4d, the modified device retained 90 % of its original efficiency after 1000 hours.

In summary, aiming to precisely manage the defects in perovskite film with inorganic passivator, a directional passivation strategy was developed by using Cu-HBT 2D

material as a passivator precursor. Cu-HBT possesses a graphene-like layer sandwiched by covalently bonded phenol functional motifs, offering the advantages of targeted modification of organic passivators and excellent stability of inorganic passivators. This novel approach involves selectively anchoring Cu-HBT to the surface of perovskite films at defective positions, and then generating Cu_2S and PbS passivators in situ to facilitate directional defect management. Additionally, the resultant passivators are p-type semiconductors with energy level matching with perovskite. As results, Cu-HBT treated PSCs exhibit remarkable improvements in humidity, thermal and light stability. This strategy also remarkably improves the average efficiency by 1.8 % and reaches the best efficiency of 23.5 %. This work not only provides a directional defect management strategy for fabricating highly efficient and stable PSCs, but also explores a new application of surface-fully-functionalized OMCs 2D materials.

Acknowledgements

We acknowledge the National Natural Science Foundation of China (22325109, 22271281, 22075116, 21975254, 22171263, 22175176, 91961115), the Natural Science Foundation of Fujian Province (2021J02017 and 2022J06032), Scientific Instrument Developing Project of the Chinese Academy of Sciences (YJKYQ20210024), and Future-prospective and Stride-across Programs of HaixiInstitutes, Chinese Academy of Sciences (CXZX-2022-JQ03).

Conflict of Interest

The authors declare no conflict of interest.

Data Availability Statement

Research data are not shared.

Keywords: Organic Metal Chalcogenides · Passivator · Perovskite · Solar Cells · Stability

[1] a) H. Zhu, Y. Ren, L. Pan, O. Ouellette, F. T. Eickemeyer, Y. Wu, X. Li, S. Wang, H. Liu, X. Dong, S. M. Zakeeruddin, Y. Liu, A. Hagfeldt, M. Grätzel, *J. Am. Chem. Soc.* **2021**, *143*, 3231–3237; b) Z. Liu, L. Qiu, L. K. Ono, S. He, Z. Hu, M. Jiang, G. Tong, Z. Wu, Y. Jiang, D.-Y. Son, Y. Dang, S. Kazaoui, Y. Qi, *Nat. Energy* **2020**, *5*, 596–604; c) G. Kim, H. Min, S. Lee Kyoung, Y. Lee Do, M. Yoon So, I. Seok Sang, *Science* **2020**, *370*, 108–112; d) J. Xu, C. C. Boyd, Z. J. Yu, A. F. Palmstrom, D. J. Witter, B. W. Larson, R. M. France, J. Werner, S. P. Harvey, E. J. Wolf, W. Weigand, S. Manzoor, M. F. A. M. van Hest, J. J. Berry, J. M. Luther, Z. C. Holman, M. D. McGehee, *Science* **2020**, *367*, 1097–1104; e) M. Jeong, I. W. Choi, E. M. Go, Y. Cho, M. Kim, B. Lee, S. Jeong, Y. Jo, H. W. Choi, J. Lee, J.-H. Bae, S. K. Kwak, D. S. Kim, C. Yang, *Science* **2020**, *369*, 1615–1620; f) J. J. Yoo, G. Seo, M. R. Chua, T. G. Park, Y. Lu, F. Rotermund, Y. Kim, C. S. Moon, N. J. Jeon, J.-P. Correa-Baena, V. Bulović, S. S. Shin, M. G. Bawendi, *Nature* **2021**, *590*, 587–593; g) Y. Xu, X. Guo, Z. Lin, Q. Wang, J. Su, J. Zhang, Y. Hao, K. Yang, J. Chang, *Angew. Chem. Int. Ed.* **2023**, *62*, e202306229.

[2] a) X. Zhang, C.-B. Nie, T.-Y. Zhou, Q.-Y. Qi, J. Fu, X.-Z. Wang, L. Dai, Y. Chen, X. Zhao, *Polym. Chem.* **2015**, *6*, 1923–1927; b) L. Wang, B. Chang, H. Li, Y. Wu, L. Zhang, L. Yin, *Angew. Chem. Int. Ed.* **2023**, *62*, e202304256; c) H. Guo, W. Xiang, Y. Fang, J. Li, Y. Lin, *Angew. Chem. Int. Ed.* **2023**, *62*, e202304568; d) W. Peng, K. Mao, F. Cai, H. Meng, Z. Zhu, T. Li, S. Yuan, Z. Xu, X. Feng, J. Xu, M. D. McGehee, J. Xu, *Science* **2023**, *379*, 683–690.

[3] a) Z. Yu, L. Wang, X. Mu, C.-C. Chen, Y. Wu, J. Cao, Y. Tang, *Angew. Chem. Int. Ed.* **2021**, *60*, 6294–6299; b) G.-B. Xiao, L.-Y. Wang, X.-J. Mu, X.-X. Zou, Y.-Y. Wu, J. Cao, *CCS Chem.* **2021**, *3*, 25–36; c) H. Min, D. Y. Lee, J. Kim, G. Kim, K. S. Lee, J. Kim, M. J. Paik, Y. K. Kim, K. S. Kim, M. G. Kim, T. J. Shin, S. Il Seok, *Nature* **2021**, *598*, 444–450; d) A. Mei, Y. Sheng, Y. Ming, Y. Hu, Y. Rong, W. Zhang, S. Luo, G. Na, C. Tian, X. Hou, Y. Xiong, Z. Zhang, S. Liu, S. Uchida, T.-W. Kim, Y. Yuan, L. Zhang, Y. Zhou, H. Han, *Joule* **2020**, *4*, 2646–2660; e) D. Li, D. Zhang, K.-S. Lim, Y. Hu, Y. Rong, A. Mei, N.-G. Park, H. Han, *Adv. Funct. Mater.* **2021**, *31*, 2008621; f) B. Chen, C. Fei, S. Chen, H. Gu, X. Xiao, J. Huang, *Nat. Commun.* **2021**, *12*, 5859–5868; g) C. Luo, G. Zheng, F. Gao, X. Wang, C. Zhan, X. Gao, Q. Zhao, *Nat. Photonics* **2023**, *17*, 856–864.

[4] a) N. Li, Y. Luo, Z. Chen, X. Niu, X. Zhang, J. Lu, R. Kumar, J. Jiang, H. Liu, X. Guo, B. Lai, G. Brocks, Q. Chen, S. Tao, D. P. Fenning, H. Zhou, *Joule* **2020**, *4*, 1743–1758; b) D. Luo, R. Su, W. Zhang, Q. Gong, R. Zhu, *Nat. Rev. Mater.* **2020**, *5*, 44–60; c) N. Li, X. Niu, L. Li, H. Wang, Z. Huang, Y. Zhang, Y. Chen, X. Zhang, C. Zhu, H. Zai, Y. Bai, S. Ma, H. Liu, X. Liu, Z. Guo, G. Liu, R. Fan, H. Chen, J. Wang, Y. Lun, X. Wang, J. Hong, H. Xie, S. Jakob Devon, G. Xu Xiaoji, Q. Chen, H. Zhou, *Science* **2021**, *373*, 561–567; d) X. Liu, X. Wang, T. Zhang, Y. Miao, Z. Qin, Y. Chen, Y. Zhao, *Angew. Chem. Int. Ed.* **2021**, *60*, 12351–12355.

[5] L. Wang, H. Zhou, J. Hu, B. Huang, M. Sun, B. Dong, G. Zheng, Y. Huang, Y. Chen, L. Li, Z. Xu, N. Li, Z. Liu, Q. Chen, L.-D. Sun, C.-H. Yan, *Science* **2019**, *363*, 265–270.

[6] Z. Fan, H. Xiao, Y. Wang, Z. Zhao, Z. Lin, H.-C. Cheng, S.-J. Lee, G. Wang, Z. Feng, W. A. Goddard, Y. Huang, X. Duan, *Joule* **2017**, *1*, 548–562.

[7] a) T. H. Han, J. W. Lee, C. Choi, S. Tan, C. Lee, Y. P. Zhao, Z. H. Dai, N. De Marco, S. J. Lee, S. H. Bae, Y. H. Yuan, H. M. Lee, Y. Huang, Y. Yang, *Nat. Commun.* **2019**, *10*, 520; b) Q. Jiang, Y. Zhao, X. W. Zhang, X. L. Yang, Y. Chen, Z. M. Chu, Q. F. Ye, X. X. Li, Z. G. Yin, J. B. You, *Nat. Photonics* **2019**, *13*, 460–466; c) J. Cao, C. Li, X. Lv, X. Feng, R. Meng, Y. Wu, Y. Tang, *J. Am. Chem. Soc.* **2018**, *140*, 11577–11580; d) Z. Fang, L. Wang, X. Mu, B. Chen, Q. Xiong, W. D. Wang, J. Ding, P. Gao, Y. Wu, J. Cao, *J. Am. Chem. Soc.* **2021**, *143*, 18989–18996; e) F. Cheng, R. He, S. Nie, C. Zhang, J. Yin, J. Li, N. Zheng, B. Wu, *J. Am. Chem. Soc.* **2021**, *143*, 5855–5866; f) R. Chen, Y. Wang, S. Nie, H. Shen, Y. Hui, J. Peng, B. Wu, J. Yin, J. Li, N. Zheng, *J. Am. Chem. Soc.* **2021**, *143*, 10624–10632; g) G.-B. Xiao, Z.-F. Yu, J. Cao, Y. Tang, *CCS Chem.* **2020**, *2*, 488–494; h) Y. Wang, T. Wu, J. Barbaud, W. Kong, D. Cui, H. Chen, X. Yang, L. Han, *Science* **2019**, *365*, 687–691.

[8] S. Yang, J. Dai, Z. Yu, Y. Shao, Y. Zhou, X. Xiao, X. C. Zeng, J. Huang, *J. Am. Chem. Soc.* **2019**, *141*, 5781–5787.

[9] S. Yang, S. Chen, E. Mosconi, Y. Fang, X. Xiao, C. Wang, Y. Zhou, Z. Yu, J. Zhao, Y. Gao, F. De Angelis, J. Huang, *Science* **2019**, *365*, 473–478.

[10] a) X. Wu, H. Zhang, J. Zhang, X. W. D. Lou, *Adv. Mater.* **2021**, *33*, e2008376; b) Y. Wen, G. E. Wang, X. Jiang, X. Ye, W. Li, G. Xu, *Angew. Chem. Int. Ed.* **2021**, *60*, 19710–19714; c) K. H. Low, V. A. Roy, S. S. Chui, S. L. Chan, C. M. Che, *Chem. Commun.* **2010**, *46*, 7328–7330; d) Y. Li, J. Shu, Q. Huang, K. Chiranjeevulu, P. N. Kumar, G. E. Wang, W. H. Deng, D. Tang, G. Xu, *Chem. Commun.* **2019**, *55*, 10444–10447; e) H. Jiang, L. Cao, Y. Li, W. Li, X. Ye, W. Deng, X. Jiang, G. Wang, G. Xu, *Chem. Commun.* **2020**, *56*, 5366–5369; f) Q.-Q. Huang, Y.-Z. Li, Z. Zheng, X.-M. Jiang, S.-S. Sun, H.-J. Jiang, W.-H. Deng, G.-E. Wang, T.-Y. Zhai, M.-D. Li, G. Xu, *CCS Chem.* **2020**, *2*, 655–662; g) M. R. Gao, Y. F. Xu, J. Jiang, S. H. Yu, *Chem. Soc. Rev.* **2013**, *42*, 2986–3017.

[11] Y. Li, X. Jiang, Z. Fu, Q. Huang, G. E. Wang, W. H. Deng, C. Wang, Z. Li, W. Yin, B. Chen, G. Xu, *Nat. Commun.* **2020**, *11*, 261.

[12] a) D. M. N. M. Dissanayake, R. A. Hatton, T. Lutz, R. J. Curry, S. R. P. Silva, *Nanotechnology* **2009**, *20*, 195205–195209; b) D. A. Dixon, J. L. Gole, *Chem. Phys. Lett.* **1992**, *189*, 390–394; c) S. C. Riha, S. Jin, S. V. Baryshev, E. Thimsen, G. P. Wiederrecht, A. B. F. Martinson, *ACS Appl. Mater. Interfaces* **2013**, *5*, 10302–10309.

[13] N. H. Hemasiri, S. Kazim, S. Ahmad, *Nano Energy* **2020**, *77*, 105292–105302.

[14] F. Cai, J. Cai, L. Yang, W. Li, R. S. Gurney, H. Yi, A. Iraqi, D. Liu, T. Wang, *Nano Energy* **2018**, *45*, 28–36.

[15] J. Cao, B. Wu, R. Chen, Y. Wu, Y. Hui, B.-W. Mao, N. Zheng, *Adv. Mater.* **2018**, *30*, 1705596–1175605.

Manuscript received: September 16, 2023
Accepted manuscript online: November 8, 2023
Version of record online: ■■, ■■

Communications

Solar Cells

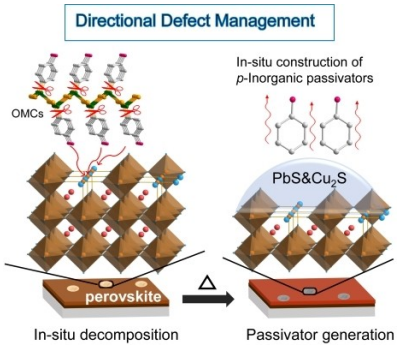

A directional passivation strategy is reported using 2D Cu-(4-mercaptophenol) as a passivator precursor, which combines the benefits of both organic and inorganic passivators through targeted modification and excellent stability, respectfully.